SPE-194313-MS

Using Land Controlled Source Electromagnetics to Identify the Effects of Geologic Controls During a Zipper Frac Operation - A Case Study from the Anadarko Basin

Mark Hickey, Oscar Vasquez, Santiago Trevino, Justin Oberle, and Drew Jones, Deep Imaging Technologies

This paper was prepared for presentation at the SPE Hydraulic Fracturing Technology Conference and Exhibition held in The Woodlands, Texas, USA, 5-7 February 2019.

Abstract

Controlled Source Electromagnetics (CSEM) is used to monitor and image a three well zipper frac operation. We examine the interaction between the completions operation and a fault zone at reservoir depth.

Using two grounded dipole transmitter lines and 350 receiver locations, 27 frac stages were monitored in the Anadarko basin for three horizontal wells. Our broadband signal is transmitted before the start of the frac stage, during the frac stage, and after the frac stage is completed. This allows us to establish a baseline image prior to the start of the frac stage and to generate a response throughout the frac. The electromagnetic data collected provides a direct measurement of the conductivity change in the subsurface caused by the hydraulic fracturing process and from this we infer fluid movement.

This case study presents the effects of a fault at reservoir depths that is intersected by the three wells and examines the possible effects of formation heterogeneities on frac fluid migration. Images produced by our CSEM method illustrate the lateral extent of the fluid, fracture azimuth, and identify reservoir heterogeneities. In addition, unlike microseismic, the CSEM method records signal generated from fluid flow in natural fractures as well as those fractures created by hydraulic pressure. As a result, CSEM allows us to infer fluid propagation and location to gauge frac behavior near and away from the fault where the fault zone is seen possibly acting as a sink and barrier. CSEM monitoring of a frac operation not only serves as a tool for monitoring and fracture diagnostic, it can also be used to identify geologic controls that can affect reservoir stimulation.

Introduction

Controlled Source Electromagnetics (CSEM) has become a commonly used tool in the exploration of offshore petroleum reserves. However, surface-based CSEM, while having been used successfully in the mining industry since the 1930s, has seen little exposure in onshore petroleum operations (Streich, 2014). Recently, knowledge and application of surface-based CSEM has grown with improvements in forward modeling, spurred on by better computers with more processing power, as well as having continuing improvements and understanding of CSEM algorithms and digital filters.

An advantage of using CSEM to monitor a hydraulic fracturing operation is that signals generated from fluid flow in natural fractures can be recorded in addition to the fractures created by the fracturing process. Imaging of the fluid when using electromagnetics is made possible by measuring the conductivity change occurring in the reservoir due to the fluid filled fracture network and does not require the use of tracers or alterations to the hydraulic fracturing fluid stream. This allows for inference of a direct measurement to observe where the fluid is flowing, and not just where fracture networks are being created.

The case study presented here focuses on the monitoring of a three well zipper frac operation with a "wine-rack" pattern and demonstrates how the CSEM imaging method shows the interaction between the frac operations and a local fault zone. The paper begins with an overview of how this CSEM method is implemented, first in theory and modeling, and then the application of the method in the field with descriptions of the technology and survey layout used for the case study. This is followed by a discussion of the case study field results and overview of frac signal behavior in relation to the fault zone. The last sections include general conclusions of the case study, and future analysis and work to be performed for the case study and for land CSEM advancement.

Method

This section discusses the physics applied for the modeling performed prior to the CSEM survey and results of the modeling. This is followed by a decription of CSEM applications, then survey design and equipment are discussed with a typical survey layout shown. The modifications necessary for the case study and an overview of data processing and imaging follow.

Theory

Through forward modeling of synthetic CSEM data, based on local ground resistivity information from well-logs taken from site, we can determine the frequencies that will have the highest signal-to-noise ratio (SNR) for a given depth and set of geologic conditions. The response of the fluid filled fracture network is dependent on several factors. These include the electrical conductivity difference between the fluid and background geological formation, electrical anisotropy of the formation, and fracture network properties such as permeability. The well casing increases the response of the fracture fluid due to mutual inductance (Commer *et al.* 2014). The frac can be viewed as a perturbation of the signal response generated by the well casing and surrounding geology. This can become more complex, however, when multiple wells, vertical wells, slant wells, and producing wells at different depths are introduced. This can be accounted for in forward modeling (Hickey *et al*., 2015). A 3D finite element mesh is created that includes casing and stage locations where a set of known EM potentials ($\mathbf{A}_p$,Ψ_p) are defined. The model then solves the Coulomb gauge Maxwell's equations in the frequency domain (Badea *et al*., 2001 and Hickey *et al*., 2015) for the electric field for the governing Maxwell's equations given by:

$$\nabla^2 \boldsymbol{A}_s + i\omega\mu_0\sigma(\boldsymbol{r})(\boldsymbol{A}_s + \nabla\psi_s) = -i\omega\mu_0\Delta\sigma(\boldsymbol{r})\big(\boldsymbol{A}_p + \nabla\psi_p\big). \tag{1a}$$

$$\nabla \cdot [\mathrm{i}\omega\mu_0\sigma(\boldsymbol{r})(\boldsymbol{A}_s + \nabla\psi_s)] = -\nabla \cdot [i\omega\mu_0\Delta\sigma(\boldsymbol{r})\big(\boldsymbol{A}_p + \nabla\psi_p\big)]. \tag{1b}$$

where $\Delta\sigma(\boldsymbol{r}) = \sigma_p(\boldsymbol{r}) - \sigma_s(\boldsymbol{r})$, is the difference between primary and secondary conductivity, ω is the angular frequency, and μ_0 is the magnetic permeability of free space. The system of equations solves for a secondary set of EM potentials ($\mathbf{A}_s$,Ψ_s) as the response to a background conductivity structure which then allows for the calculation of the secondary electric field, $\mathbf{E}_s$. Analysis of the expected secondary response in the presence of the frac fluid aids in survey layout design and interpretation and allows for further experimentation in model space for applications in the field.

Modeling

To determine the expected response of fluid injection for the CSEM system the model begins with well-log data which is smoothed to determine a set of conductive model layers (Fig. 1A) of the study area. The number of conductive layers used is determined by the amount of computational resources available. Large changes between consecutive minima and maxima for layer boundaries are of interest. These layers are used to create a 3D finite element mesh with external programs such as Tetgen (Hang Si 2015) as shown in (Fig. 1B). Local mesh refinement is used around the source, receiver area, conductive boundaries, and target boundaries to increase numerical accuracy. Additionally, to account for the mutual inductance between fracture fluid and well casings, the horizontal segment of each well casing is represented in the model at appropriate depth and spacing (Fig. 1C). To reduce the number of nodes in the mesh, the well casing is included in a 35 ft^3 volume whose conductivity is an average between the well casing and background conductivity. Our source is a long grounded horizontal electric dipole at the surface with a current of 1 A to generally represent the current applied to each frequency band in the field data. We investigate frequency responses from 1 Hz to 1000 Hz with 10 steps per decade and interpolate in-between frquencies. For frequency bandwidths that need further investigation, we can run more models with finer frequency steps in the bandwidths of interest. For each frequency step, we determine the response of the 4 horizontal casings and separately, the 4 horizontal casings and injection fluid. This allows us to subtract the difference to determine the ideal frequency range of the expected fluid response.

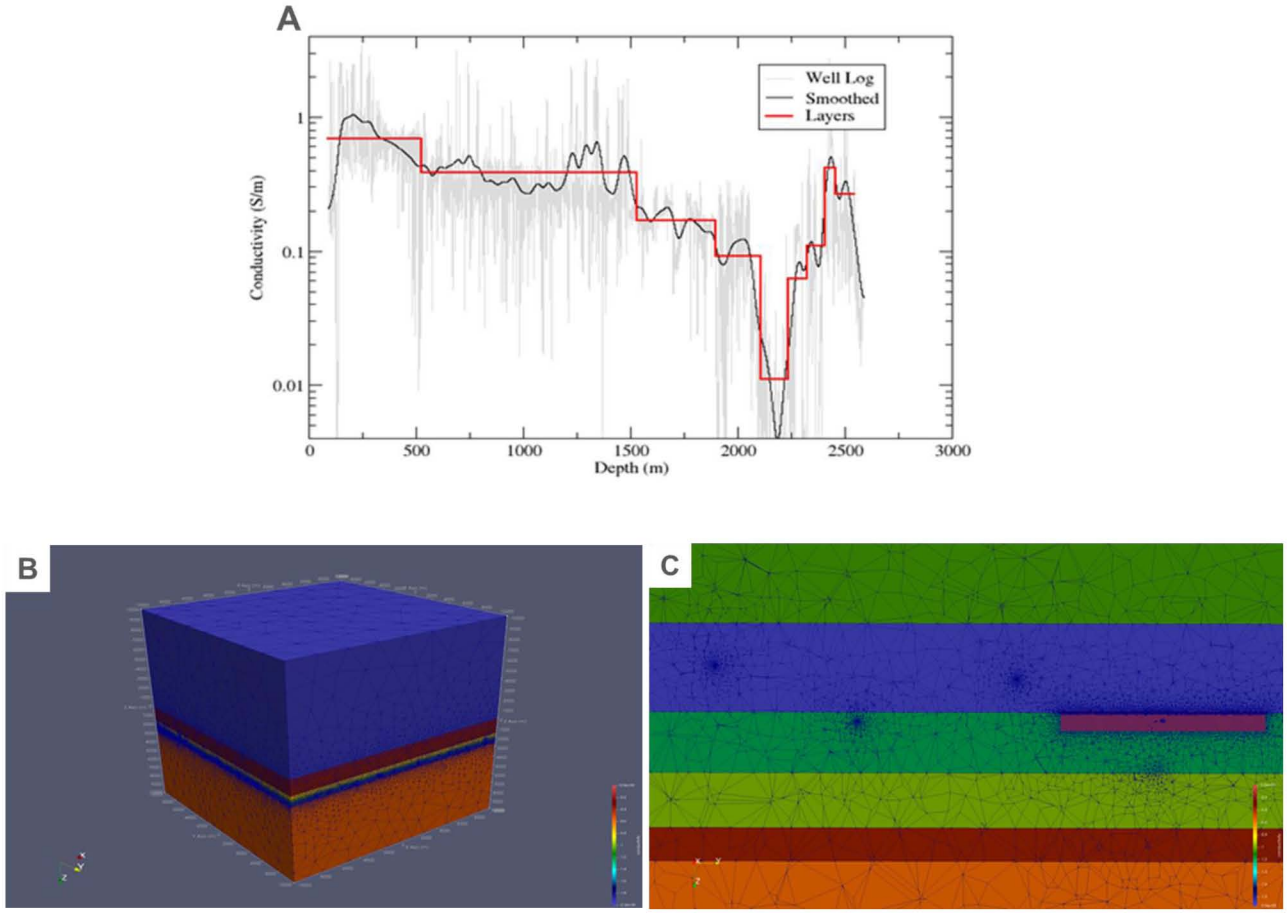

Figure 1—(A) Well-log with model layers (B) Model overview (C) Gun-barrel view of casing locations where casing locations are can be seen by the concentration of mesh points

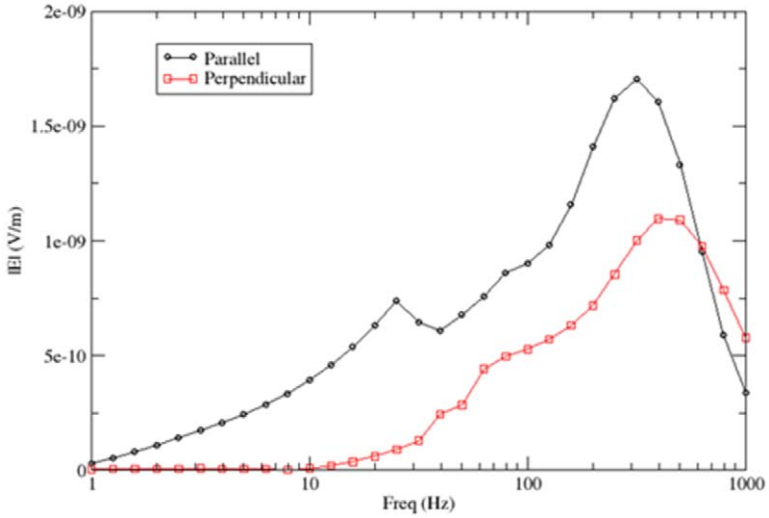

Figure 2—Result of the model for the case study

The results for our case study, for a point at the surface and directly above the fluid extent, is shown in Figure 2. As can be seen, the ideal frequency, with the highest SNR for the given conditions, is about 300-350 Hz for the parallel components and about 400Hz for the perpendicular components. With that said, a response will be shown on all frequencies for the parallels and a range of about 10-1000 Hz for the perpendiculars.

Uses of Land CSEM

Land CSEM also has applications to other petroleum fields aside from the frac monitoring presented in this case study. Due to the ability to gauge the lateral extent of the frac fluid, CSEM is ideal for detecting frac hits. This can similarly be applied to hazard assessments, particularly in locating aquifers, and monitoring operations to ensure the fracturing process does not interfere with the state of the aquifer. In addition, for areas consisting of carbonates, the risk of operating wells near formations containing large void spaces can also be assessed using CSEM.

This method has also been applied to Flow Back and Enhanced Oil Recovery (EOR) operations. For EOR, thermal, gas, or chemical injection downhole is used to stimulate crude oil production. As these fluids have different resistive properties, it is possible for CSEM to detect the conductivity changes in the subsurface with respect to the surrounding formation and fluid in place. As in the detection of the conductivity change for EOR, CSEM can be similarly used for flowback operations. With CSEM, the change in conductivity between water and oil production can be detected to monitor the success (or failure) of the frac operation. This is done by showing the main fluid channels as they open and close during the flowback process, thereby show the major drainage zones of the monitored area.

Survey Design

The CSEM source is a long, grounded wire that delivers a broadband Pseudorandom Noise (PRN) signal that can go up to 64 frequency steps per 1 Hz or higher. The PRN code allows for removal of surface and near surface re-radiation sources such as pipe lines, rail lines or other local metallic structures. Receivers, consisting of two grounded wire sensors, sample the transmitted signal at a high sample rate within nanoseconds at a SNR of −140 dB where we have determined that to detect the response due to injection of the hydraulic fracturing fluid, a CSEM system needs −120 dB of SNR (Hickey *et al.*, 2015). Additional SNR can be gained through processing methods. The transmitter wire is placed parallel to, and directly above the lateral of the wellbore of interest with rows of receivers alongside. The transmitter can be up to 5000 feet in length, depending on the well being monitored. Receiver wires are placed offset the transmitter

line at orientations perpendicular and parallel to the transmitter to measure two channels (Ex, Ey) and are up to 200 feet (ft) in length. This setup can be adapted when there are multiple horizontal wells of interest as in the case study, and survey design is careful to avoid areas with high amounts of EM noise i.e. drill pads, residences, highways, etc where the goal of the survey layout is to be as dense as possible while avoiding these sources of noise. An EM receiver can be placed between 50 to 100 ft away from a 3 phase noise source however, such as power lines or power gnerators, as the 3 phase arrangement is designed to reduce EM radiation. Further, an example layout is shown in Figure 3.

Figure 3—Example of a survey layout

Using two grounded transmitter lines and 350 receiver locations consisting of two sensors per location, 27 frac stages were monitored in the Anadarko basin for three horizontal wells presented as wells X, Y, and Z (Fig. 4). The transmitter (TX1) is placed above the lateral of the target well (well X). The two wells on the eastern side, Y and Z, have a transmitter (TX2) placed in between the wells running parallel to them. The lake located in between wells Y and Z results in the absence of some receiver coverage.

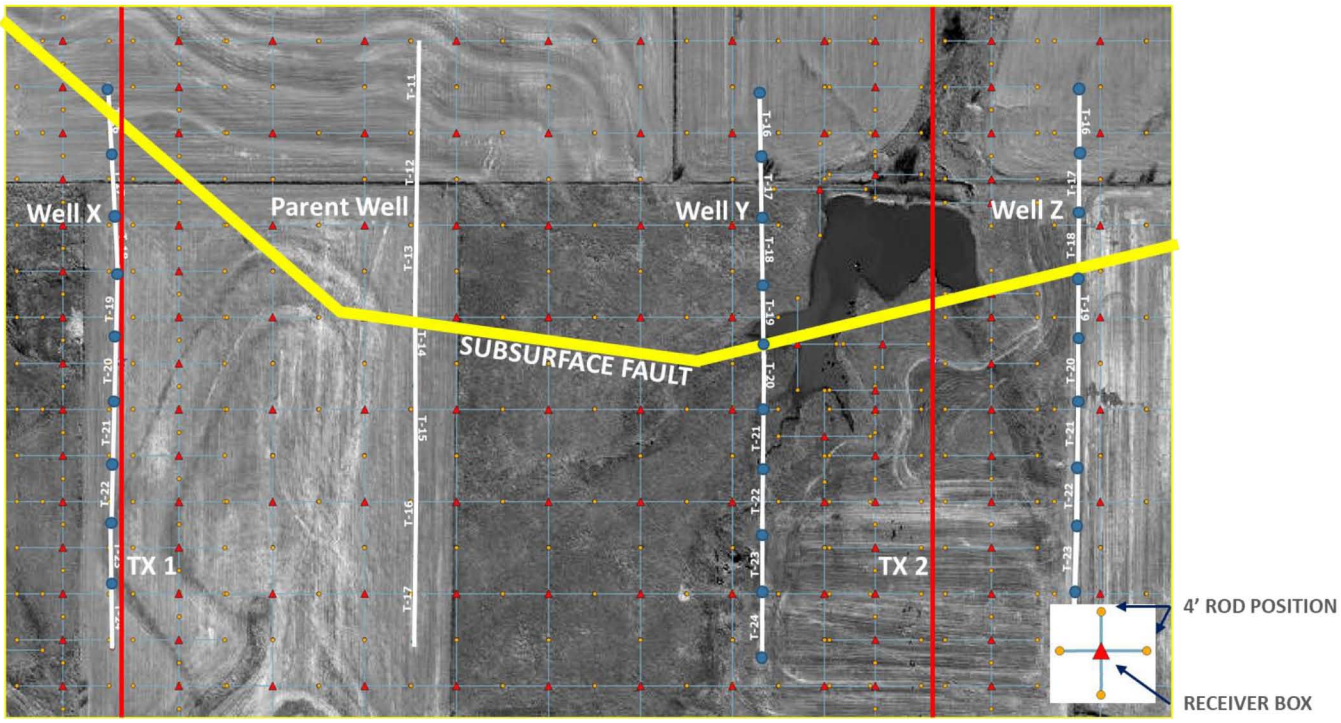

Figure 4—Actual survey design for case study of Anadarko Basin. The circles on the wells represent stages

The PRN code transmitted for the case study survey is 32 seconds in length and transmits 8191 bits. This gives a frequency bandwidth of 1 Hz to 210 Hz and a per hertz frequency step of 1/32 Hz. This gives us a per frequency bandwidth of 32 frequencies per hertz and over 6500 total frequencies. The broadband signal is transmitted before, during, and after the frac stage to establish a baseline image and to generate a response throughout the fracturing process (Fig. 5). After the data is recorded, it is checked for quality, processed, then imaged.

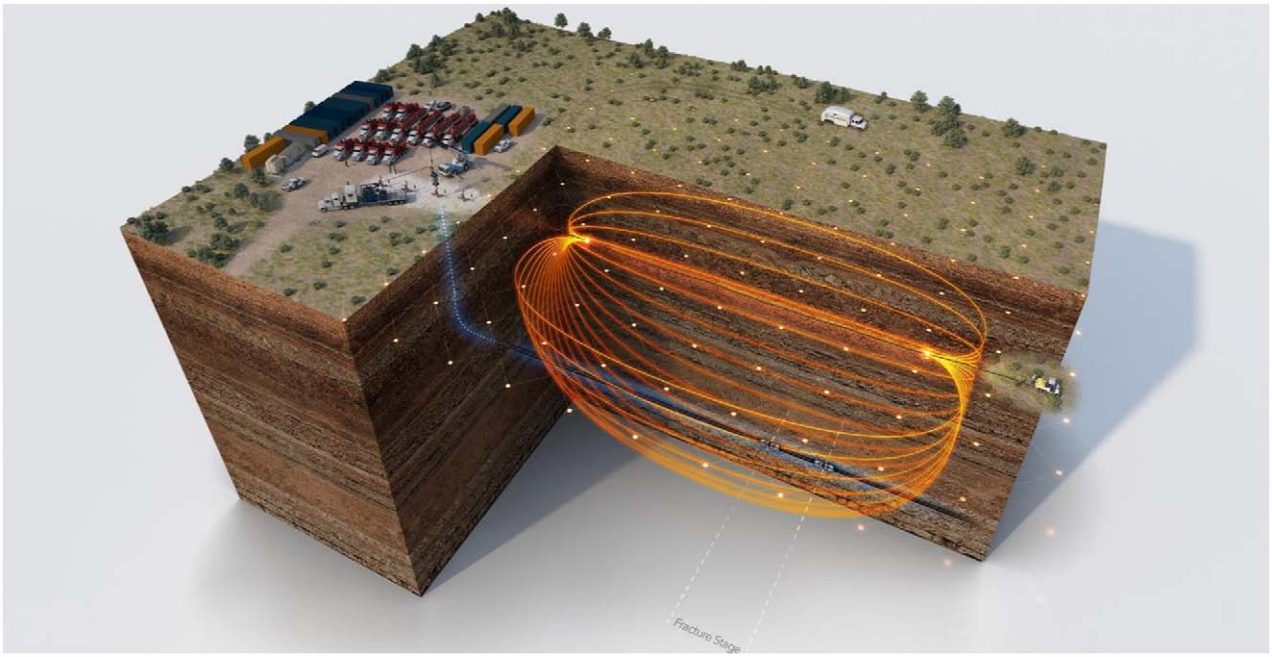

Figure 5—Schematic of surface electromagnetics transmission while fracking

Processing and Imaging

Processing and imaging are performed using in-house software. The data is recorded and initially processed in the time domain before being transformed into the frequency domain for imaging. Processing of the data in the time domain primarily consists of eliminating receivers with missing or irrecoverable data and converting the data into frequency using a windowed Fast Fourier Transform (FFT). To increase the SNR, multiple time windows are included in the FFT and act as stacking of data. Additional filters can also be applied in time to increase SNR prior to data transformation if needed. Imaging of the data is then performed in the frequency domain by looking at either the amplitude ratio of the received data to the transmitted signal or the phase difference of the received data to the transmitted signal. Viewing the data across frequencies allows for further observations of which receivers are affected most by noise. If noise is present, filters can be applied to reduce the noise, and in some cases, additional receivers need to be removed. This is done by comparing images produced at different frequency ranges as well as looking at their amplitude and phase across time for all frequencies. There are some frequency ranges, such as 60Hz that are always very noisy and must be avoided completely.

In addition, for the case study presented, the parallel sensors appeared to dominate the signal of interest due to an apparent coupling of signal with the transmitter. This dominant signal can be removed because of the cyclic nature of the PRN code transmitted. However, in the presence of strong subsurface signal in the perpendicular sensors and because bringing the two axis signals into the same range for display purposes requires time and care the parallel sensors were removed from imaging. It is always preferred to include both axes in the created image and recent work has shown that phase data is more amenable to this goal.

The baseline signal response prior to the start of the frac stage, "pre-frac", is assumed to stay the same throughout the frac. With this assumption, the "pre-frac" signal is subtracted from the frac signal and the difference provides the only changes taking place subsurface, the apparent conductivity change due to the addition of hydraulic fracture fluid filling fractures and creating connections. Afterwards, the data can be further smoothed, and cross-field noise can be removed if needed. The result is then shown in plan view where the response is summed over a selected frequency range. Showing a 2D representation of the fluid movement from the signal allows for a quicker processing time than showing an inverted 3D image. This allows for quicker decision making in the field if necessary.

Case Study

Controlled source electromagnetics (CSEM) was used in the Anadarko Basin to monitor and image a three horizontal well zipper frac operation with well geometry in a "wine-rack" pattern. The "wine-rack" pattern consists of offset wells at depth (Fig. 6A) where the well array is designed to optimize frac production in different formations or zones. The zipper frac technique involves the fracturing of adjacent wells in an alternating sequence (Fig. 6B).

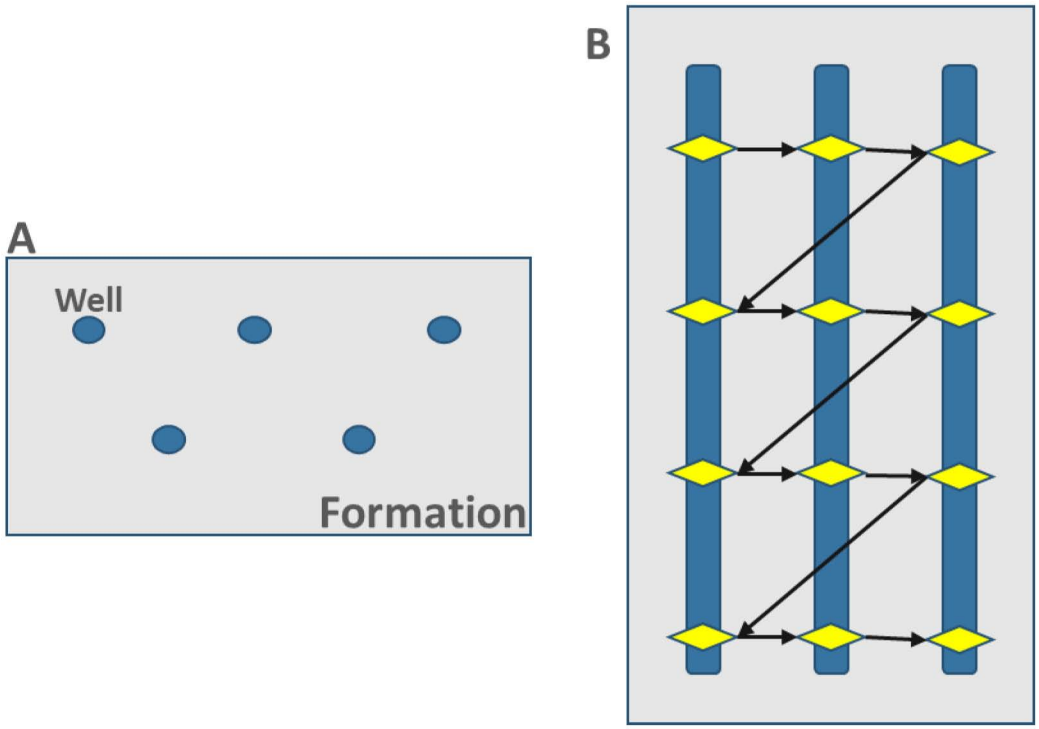

Figure 6—(A) Side view of wine rack well array and (B) map view of one type of example zipper frac operation with diamonds representing frac stages

Each stage was recorded for 2 hours where the wells, as previously mentioned, have been labeled as wells X, Y, and Z. The frac zipper sequence alternated each stage beginning with well X, followed by a frac stage at well Z until the outer wells had done a set number of stages. The same number of stages were then completed on well Y. This paper presents the results of these frac stages per well by their designated frac order. We examine the interaction between the frac operation and a fault zone at reservoir depth, that has been labeled as "FAULT ZONE" and outlined with a translucent yellow line in the plan view images presented for each well. The lateral extent and direction of the interpreted frac signal are outlined, and arrows are used to indicate frac azimuth and half-length direction. The observed frac signal is viewed in terms of signal amplitude ratio and is interpreted to be a direct response of the hydraulic fluid entering the formation.

Well X

We begin with well X at a stage located just south of the fault zone. The frac signal shows a half-length of 450 ft towards the east at an angle of 90 degrees. However, the maximum extent of the signal for the stage, highlighted by the red outline in Figure 7, trends about 45 degrees northeast and appears to approach the parent well. This observation is revisited in a later section as an examination of why the signal migrated towards the parent well is set for future analysis.

The end of frac signal of the following stage (Fig. 8) is comparable in size to the previous, with a lateral extent of 450 ft, but trending at 63 degrees northeast. The faded outline shown in the background is the end of frac signal for the previous stage. The third stage (Fig. 9), again, shows an extent of 450 ft, but with a 36-degree angle from north.

Overall, the first three stages recorded from well X exhibited similar frac half lengths, and frac azimuth appeared to be directly affected by the fault zone as frac azimuth trended towards the direction of the fault zone with respect to stage location. This produces implications that the fault zone influenced the migration of the frac fluid during these stages. An interpretation of this behavior is that the hydraulic fluid was barred from its target formation by the fault zone and stimulated a different part of the formation. This different part of the formation was then restimulated by the second and third frac stages.

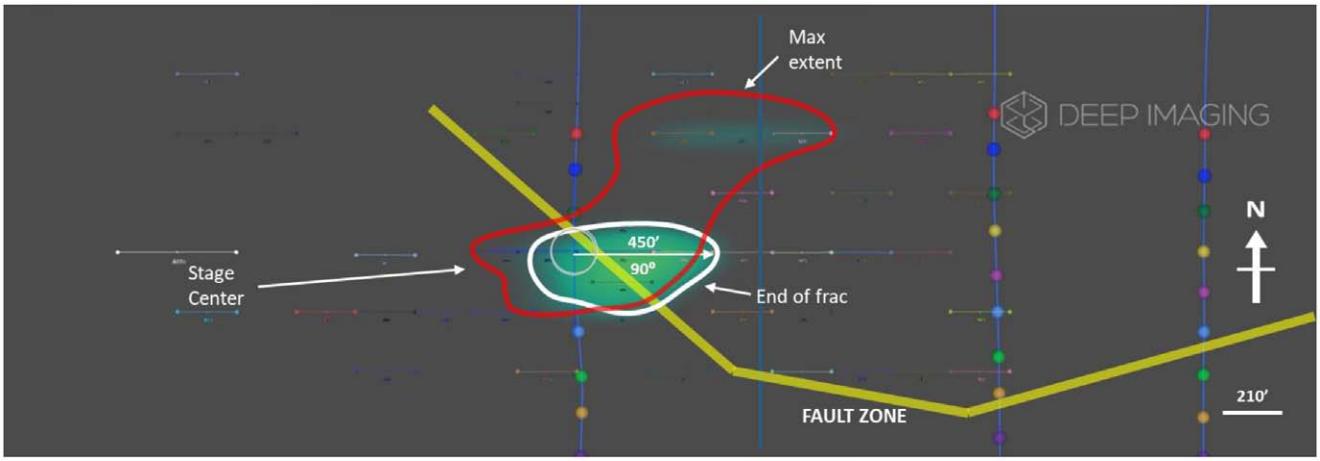

Figure 7—Resulting EM signal of the first stage recorded from Well X highlighting the end of frac azimuth, half-length, and max extent reached during pump phase

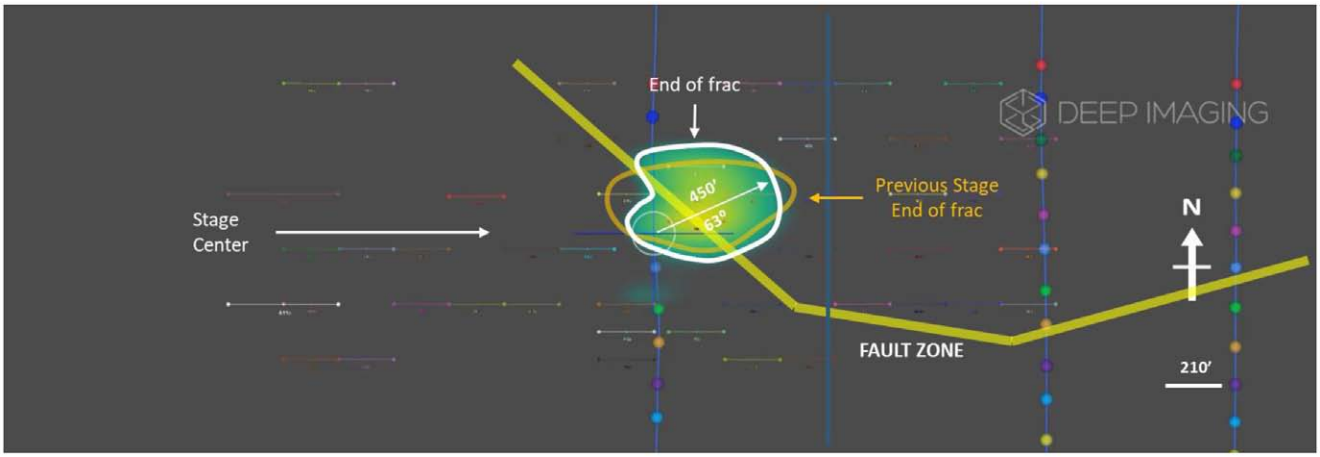

Figure 8—Resulting EM signal of the second stage recorded from Well X highlighting the end of frac azimuth and half-length overlaid on the end of frac of the previous stage

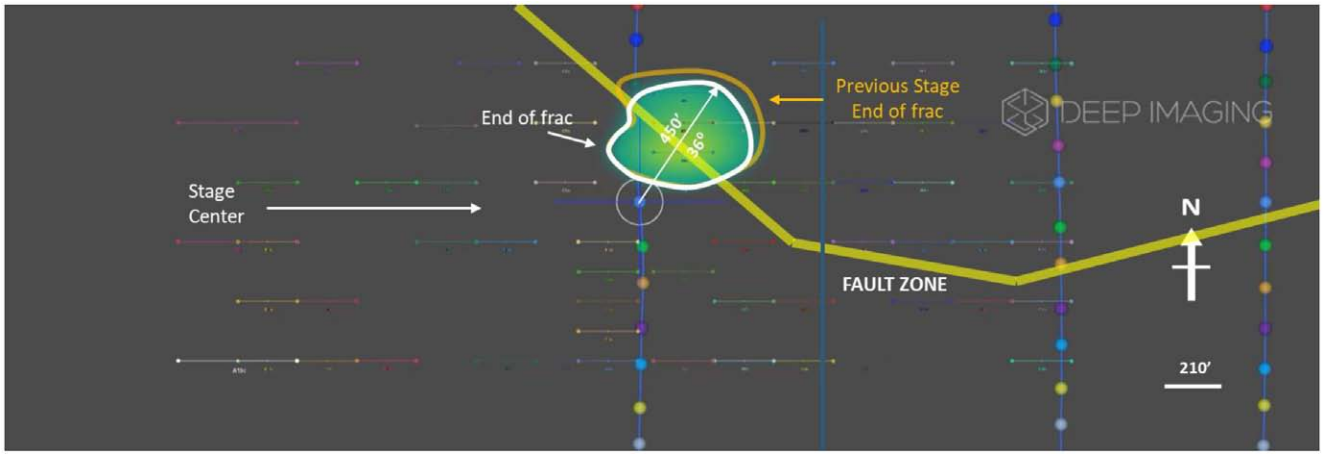

Figure 9—Resulting EM signal of the third stage recorded from Well X highlighting the end of frac azimuth and half-length overlaid on the end of frac of the previous stage

These observations no longer pertain for frac signals of stages further south along well X. As stage location moves further south and away from the fault zone, the frac azimuth appears to correct, aligning with the expected regional stress direction of the area, as the end of frac reaches an extent of 300 ft to the

east and 230 feet to the west with a frac azimuth of 112 and 281 degrees respectively in Figure 10. The lateral extent increases further with the following stage (Fig. 11), reaching a frac extent of 650 ft west of the well and 475 ft east of the well with frac azimuth of 273 and 93 degrees respectively. The azimuth and extent of the stage shown in figure 11 is more aligned with the expected regional stress direction.

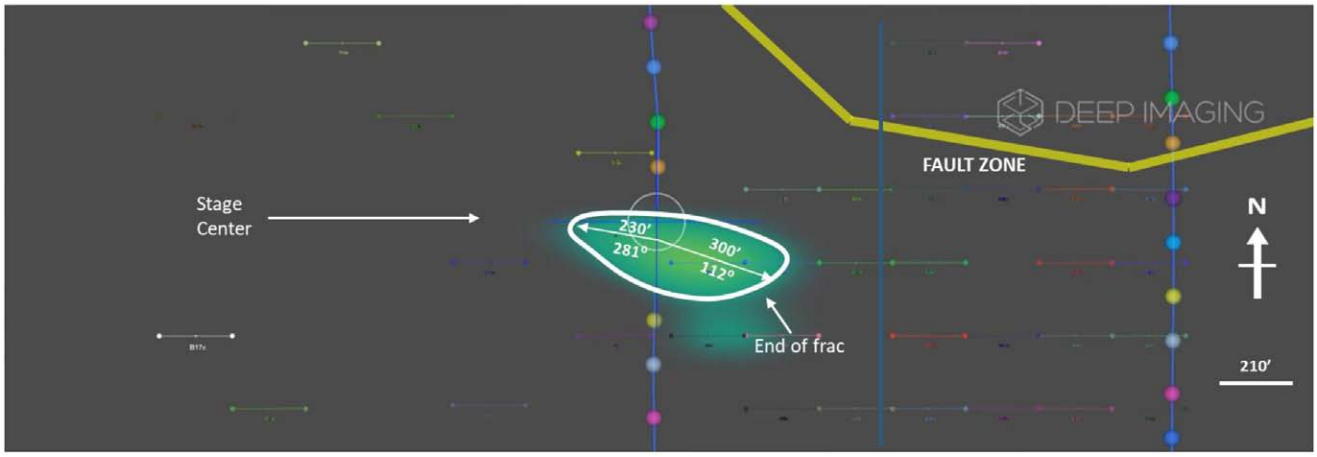

Figure 10—Resulting EM signal of the fourth stage recorded of Well X highlighting end of frac azimuth and half-length. No end of frac is shown for the previous stage due to lack of receiver information

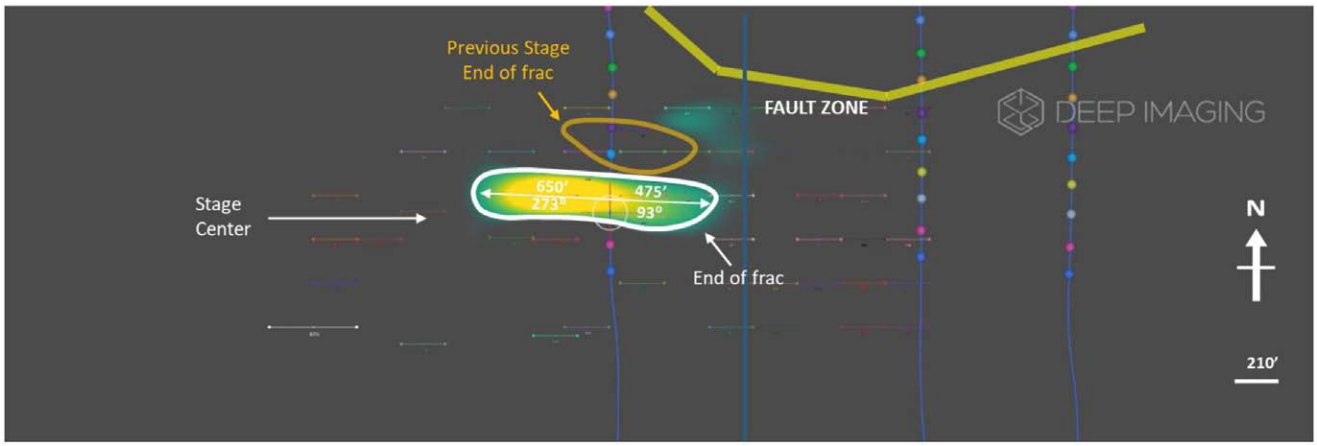

Figure 11—Result of the fifth stage recorded of Well X highlighting the end of frac azimuth and half-length of the fifth stage overlaid on the end of frac of the previous stage

Well Z

As previously mentioned, there is no receiver coverage between wells Z and Y in the area where a lake is present (Fig. 4). This lack of receiver coverage may have been the cause of signal loss in certain areas near the stages monitored (Fig. 12-16). The first two stages monitored from well Z are located north of the fault zone. The first stage monitored (Fig. 12) shows a frac half-length of about 500 ft and azimuth of 100 degrees to the southeast. Figures 13A and 13B show the resulting maximum extent and end of frac signal for the proceeding stage.

Prior to dissipation of the frac signal near the end of the stage, the frac azimuth is estimated to be a 267-degree angle and the frac half-length is 850 ft. During this stage, there was a 15-minute shut-in period thirty minutes after frac initiation. This resulted in a drawdown of fluid flow following a reduction of proppant concentration, prior to the pumps returning to regular flow. This drawdown complicates imaging as it essentially removes the initial baseline established prior to flow, and a new baseline time had to be

chosen for the second half of the stage. As there is still flow, although minimal in comparison to flow during fracturing, choosing a new baseline runs the risk of removing real data.

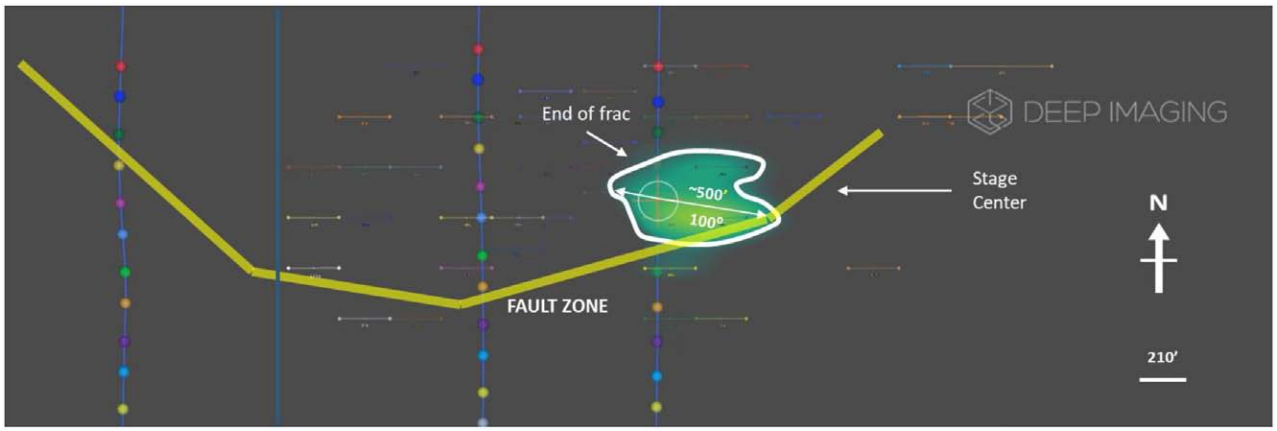

Figure 12—Result of the first stage recorded of Well Z highlighting the end of frac azimuth and half-length

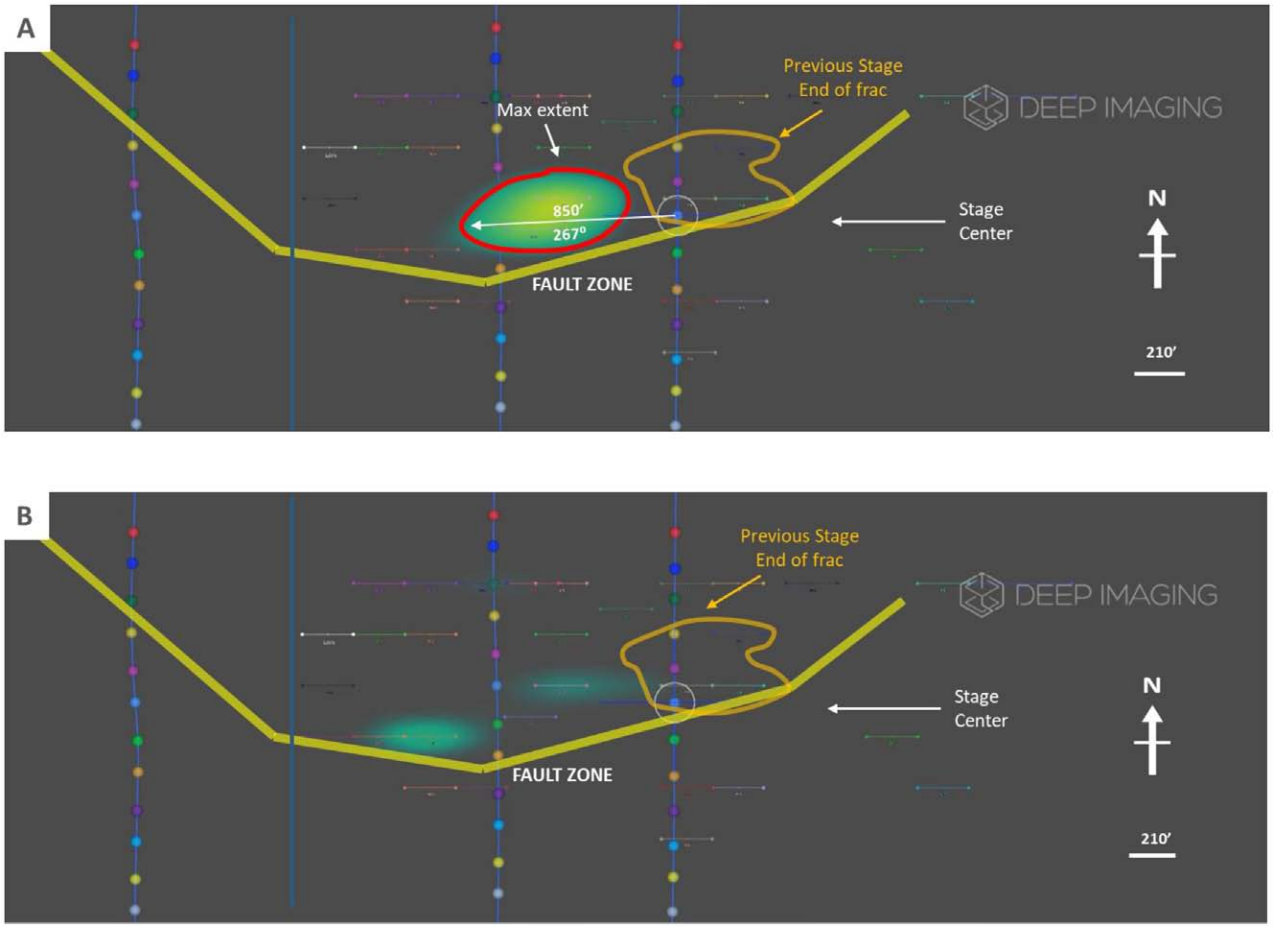

Figure 13—(A) Resulting EM signal of the second stage recorded from Well Z highlighting the max extent azimuth and half-length overlaid on the end of frac of the previous stage and (B) the end of frac signal loss

These first two stages are of interest because of their vicinity to the fault zone where the hydraulic fluid for either stage does not appear to cross the fault zone. The frac signals for both stages behave differently from each other as the frac signal produced by the second stage drifts towards well Y before dissipating. As there is some signal seen in Figure 13B, there may be a possibility that the low amplitude is a result of the

subtraction taken during fluid drawdown and that the frac was successful in stimulating the zone between wells Y and Z. This may have been caused by the fault zone acting as a barrier or may have been the result of the of lack of receiver coverage south of the fault zone (Fig. 13B).

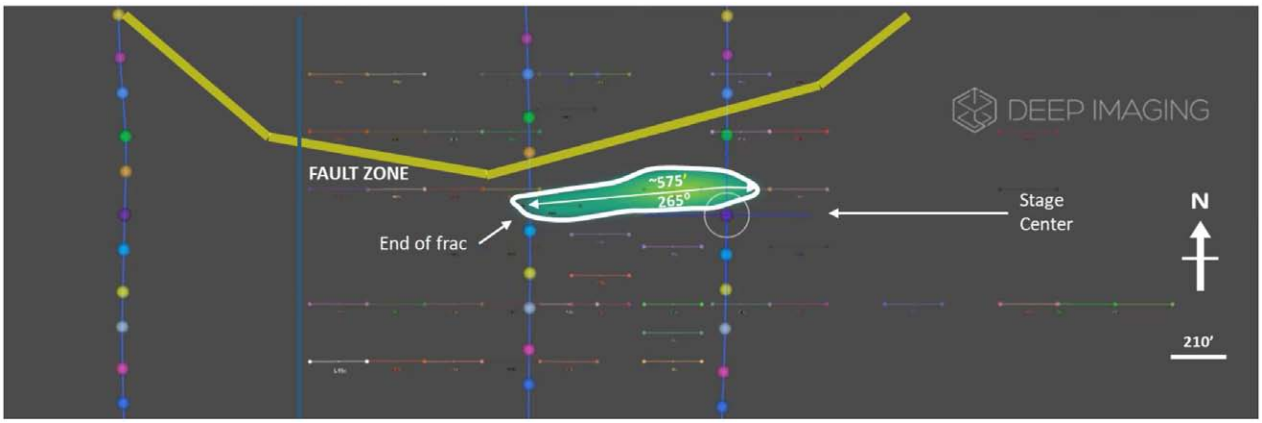

Figure 14—Resulting EM signal of the third stage recorded from Well Z highlighting the end of frac max extent azimuth and half-length

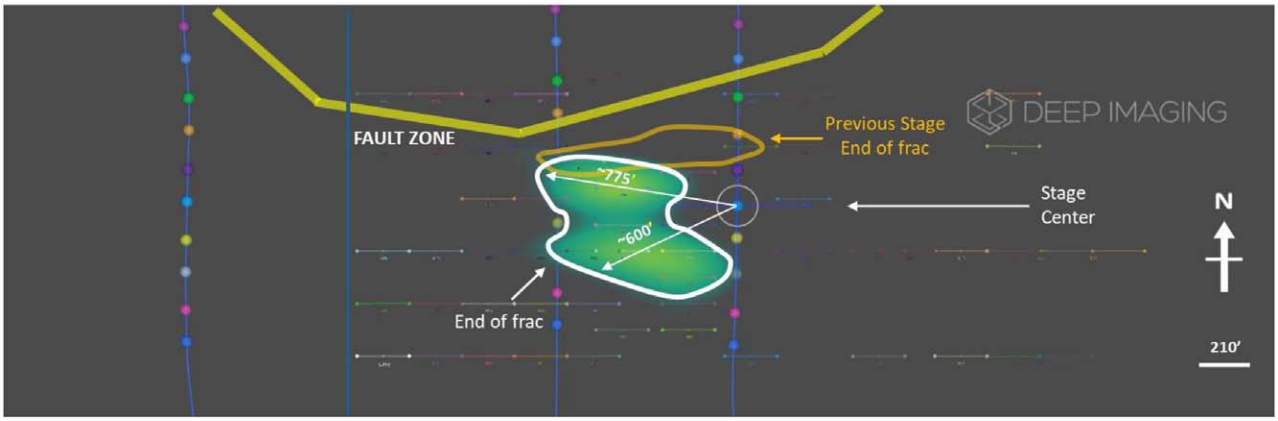

Figure 15—Resulting EM signal of the fourth stage recorded from Well Z highlighting the end of frac azimuth and half-length overlayed on the end of frac of the previous stage

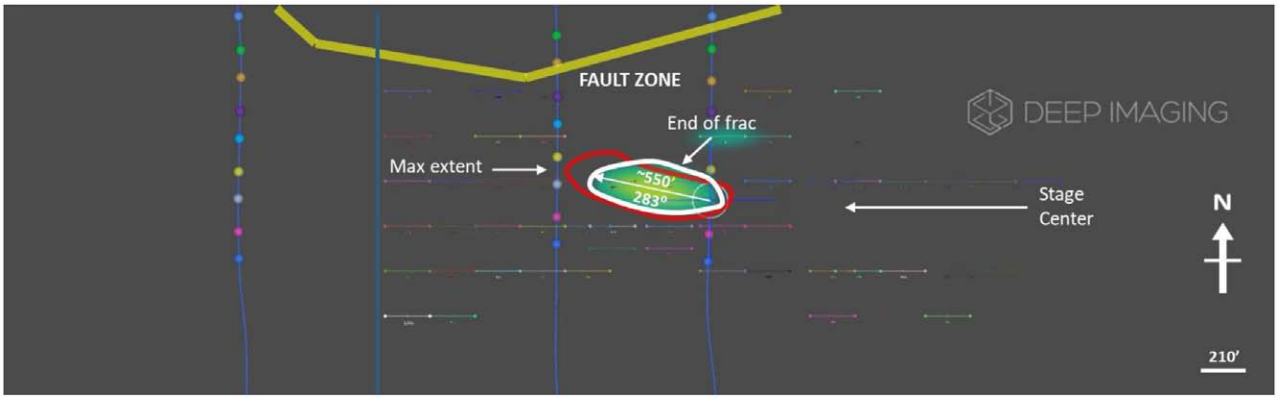

Figure 16—Resulting EM signal of the fifth stage recorded from Well Z highlighting the end of frac azimuth and half-length overlaid on the max extent of that frac stage

For the following stage (Fig. 14), further south and away from the fault zone, the frac azimuth is 265 degrees southwest with a frac half-length of about 575 ft. The next stage shows signal traveling towards the adjacent well. As there appear to be two distinct signals, no frac azimuth is calculated, but frac lengths have

been determined to be 775 ft trending northwest and 600 ft southwest (Fig. 15). The last stage monitored shows a frac azimuth of 283 degrees northwest and length of 550 ft (Fig. 16). The last three stages do not appear to be influenced by the fault zone.

Well Y

The first three locations monitored are north of the fault zone. The first stage monitored gives signal producing frac half lengths of 950 ft with a frac azimuth of 101 degrees southeast and additional frac half-length of 525 ft with a frac azimuth of 255 degrees southwest (Fig. 17). Frac signal from the first stage migrates towards well Z indicating possible frac network growth. In Figure 18, the signal crosses the fault zone as it extends towards well Z again. The frac half-length is estimated to be 925 ft with a frac azimuth of 100 degrees southeast. The signal in the third stage (Fig. 19) has estimated frac lengths of 475 ft and 675 ft trending 263 degrees southwest and 54 degrees northwest. This appears to reenter previously stimulated zones above the fault as it migrates north and does not cross the fault zone.

The fault zone may have acted as a barrier during the first and third stages that forced hydraulic fluid to restimulate previously fractured areas in the formation located further north. The behavior observed in well Y's third stage can also be interpreted as a pressured-up zone near well Z being affected by a newly created fracture network as a result of well Y's third stage. If this is the case, the pressure is released near well Z and a change in conductivity can be measured as it propagates north towards well Z from the third stage at well Y.

The final stage recorded for this well shows a frac azimuth trending 90 degrees east with a frac half-length of 500 feet (Fig. 20). Figure 20 shows the frac signal overlaying the result of the fourth stage recorded from well Z. The overlap indicates further growth of the fracture network.

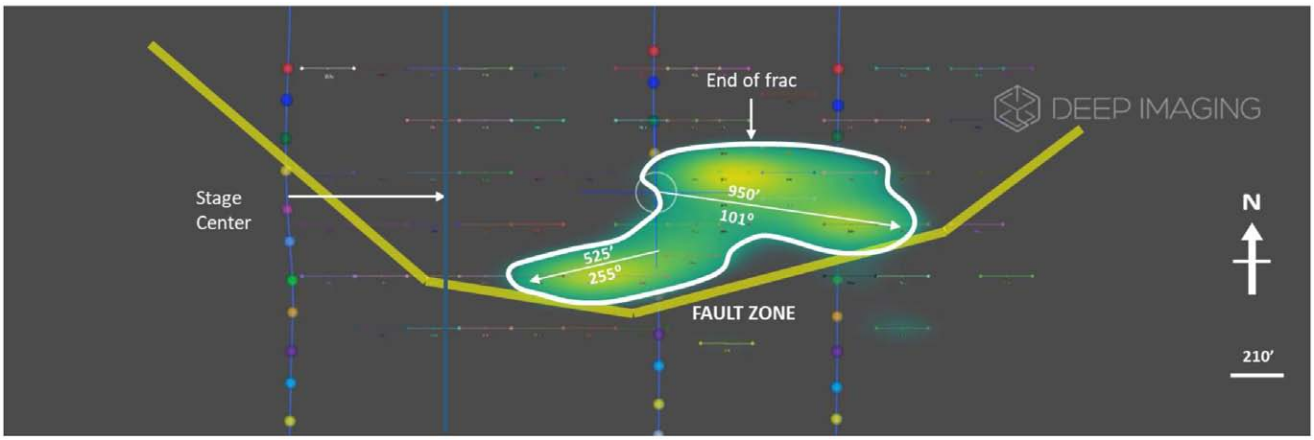

Figure 17—Result of the first stage recorded of Well Y highlighting the end of frac azimuth and half-length

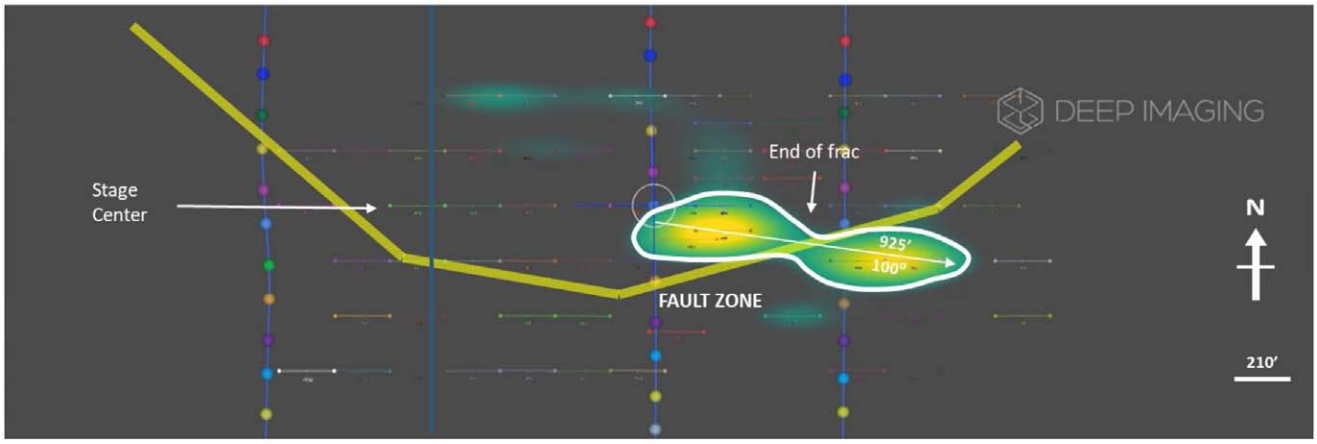

Figure 18—Result of the second stage recorded of Well Y highlighting the end of frac azimuth and half-length

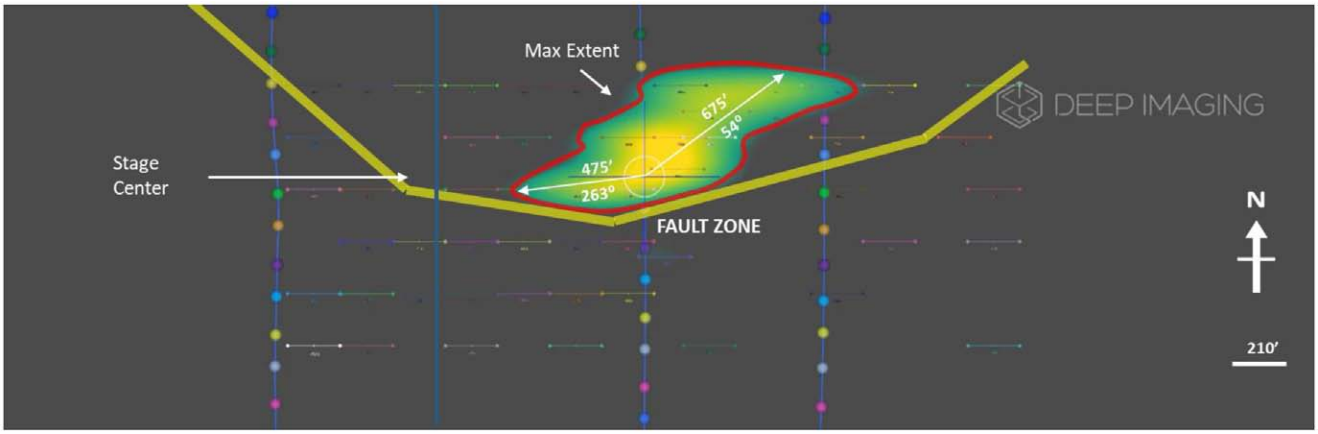

Figure 19—Result of the third stage recorded of Well Y highlighting the end of frac azimuth and half-length

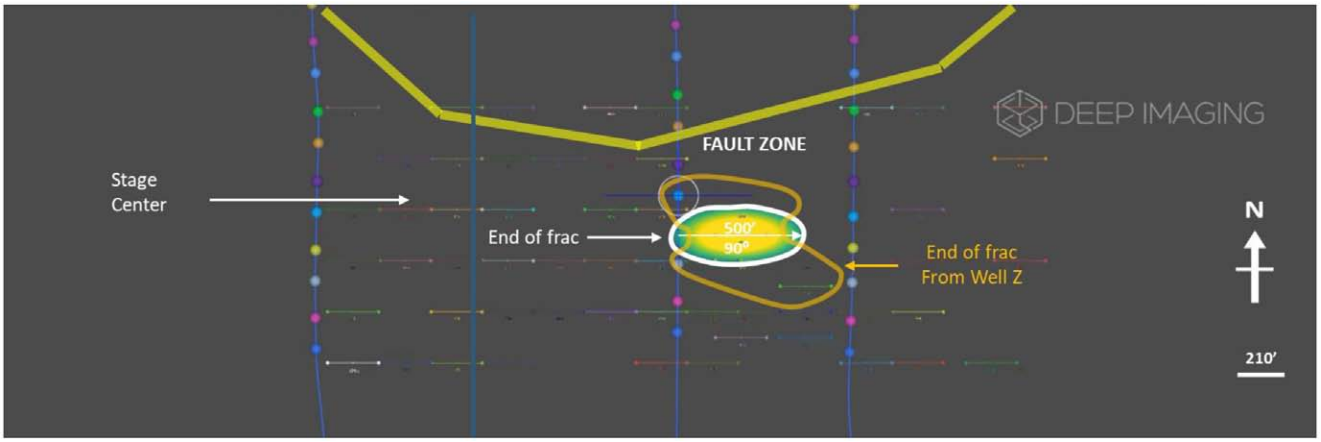

Figure 20—Result of the fourth stage recorded of Well Y highlighting the end of frac azimuth and half-length overlaying the end of frac signal from an adjacent frac stage of Well Z

Conclusions

This case study presents the effects of a fault zone at reservoir depths that is intersected by three wells. The first three stages recorded from well X were located south of the fault zone. Frac signals for all three stages exhibited similar frac half lengths. Frac azimuths for the first three stages also trended more northward towards the fault zone as stage locations proceeded further south of the fault zone. Due to the frac signal behavior observed during the first three stages recorded for well X, it is implied that the fault zone interfered

with the frac operation. Moving further south in later stage locations along well X, the influence of the fault zone is no longer observed as frac half-length and azimuth widen trend more towards the expected regional stress direction of the area.

The first two stages monitored from well Z and the first 3 stages in well Y are located north of the fault zone. The frac signal for those stages, aside from well Y's second stage (Fig. 18) did not cross the fault zone. There are two interpretations made about the frac signal interactions between wells Y and Z in relation to not crossing the fault zone and producing fracture network growth. The first is that there was restimulation in zones between both wells resulting in fracture network growth, but there was no southward fluid advancement due to the fault acting as a barrier. In the case of the frac signal's northward growth in the third stage for well Y (Fig. 19), the interpretation is there was a pressurized zone caused by an earlier stage in well Z that was stimulated by activity in well Y and created a new fracture network trending northward. The fault zone again, may have acted as a sink or barrier in this case. It is also possible that the lack of receiver coverage south of the fault zone led to signal loss in the area preventing any image below the fault zone from being produced. If this is the case, then whether the fault zone acted as a sink or barrier in this portion of the frac operations remains in question. As experienced in well X, as stage locations are further south from the fault zone for wells Y and Z there appears to be no effects caused by the fault zone on the frac signal.

Overall, images produced by our CSEM method illustrate the lateral extent of the fluid, fracture azimuth, and allow us to see the changes in frac behavior and extent across multiple stages. CSEM can be used to gauge the effects of geologic controls such as fault zones, as can be observed with the changes in signal due to fault zone vicinity in the case study. The fault zone may act as a sink or barrier for the fluid as is observed in the results. As the stages move further away from the fault zone, the frac corrects in azimuth and lateral extent increases in the expected direction of the regional stress. Identification of geologic controls that may improve or inhibit stimulation provides engineers more information needed for developing procedures to avoid potential geologic hazards, and optimize stage spacing, well spacing, and well production. Future works in estimating fluid migration at different depths from target and implementation of real time are discussed below.

Future Work

In the first frac recorded for well X, frac activity is seen NE of the stage center adjacent to the parent well (Fig. 10). The initial interpretation was the frac had broken through to the depleted zone around the parent well. More information from the well site leads us to believe that the frac may have broken through to a shallower porous sand layer which offered less resistance to the frac fluid spreading. There was a significant microseismic event at a shallower depth that corresponds to the location of the EM response observed adjacent to the parent well. Future research will include investigating ideal frequency ranges to observe this type of activity and integrating microseismic data. Finding the ideal frequencies to view such activity can be found in modeling, as it is already used to estimate frequencies required to find the maximum signal change at target depth due to conductivity changes. These frequencies also change with target depth and formation resistivity. With the information available for the study area, a model targeting the above formation can be used to predict target frequencies where optimizing such models can help in inferring a three-dimensional image of the fluid flow with depth.

Another goal to achieve is real time data acquisition. Currently the turn around time on data acquisition and processing is about 12 hours after the frac stage ends, mostly due to the large amount of data that requires transfer using secure digital (SD) cards. This would expand the field of surface-based CSEM by allowing quick detection of frac hits and screen outs during frac operations leading to more effective prevention of operation delays, or allowing for real-time decision-making using diverters or change in pump times. This can be done with the application of Wi-Fi and communication across servers allowing for fast transfer of information from the field to the processing unit. CSEM can easily detect unwanted fluid migration because

it can infer a direct measurement of the frac fluid. There are many challenges with real time CSEM, such as the tremendous size of the data collected, but as technology gets better, this becomes much more achievable.

Nomenclature

A. $\boldsymbol{E_p}$ - primary electric field
B. $\boldsymbol{E_s}$ - secondary electric field
C. $\nabla\cdot$ - the divergence, which calculates the outward flux of a point in a vector field
D. ∇^2 - the Laplacian operator, which represents a deviation of a field with respect to a point
E. $\boldsymbol{A_p}$ - the primary vector potential
F. $\boldsymbol{A_s}$ - the secondary vector potential
G. ψ_p - the primary scalar potential
H. ψ_s - the secondary scalar potential
I. σ_p $\boldsymbol{(r)}$ - primary conductivity response with respect to the medium
J. σ_s - secondary conductivity response with respect to the medium
K. i – a representation of an imaginary component
L. μ_0 - magnetic permeability of free space equal to the value of 4πE-7
M. ω - angular frequency which is also equal to to 2π*frequency
N. $\Delta\sigma(\boldsymbol{r})$ - difference between primary and secondary conductivity with respect to r
O. Frac hit - an interwell communication event where an offset well, often termed a parent well, is affected by the pumping of a hydraulic fracturing treatment in a new well (child well)
P. Screen-out - a condition that occurs when the solids (proppant) carried in a treatment fluid creates a bridge across restricted flow area causing a rapid rise in pump pressure
Q. Wine-rack - well geometry where adjacent wells are offset at depth
R. Zipper frac - a frac operation where frac stages alternate between adjacent wells in a predetermined order.

References

Badea, E. A., Everett, M. E., Newman, G. A., & Biro, O. (2001). Finite-element analysis of controlled-source electromagnetic induction using Coulomb-gauged potentials. *Geophysics*, **66**(3), 786–799

Commer, G., Hoversten, M., and Um, E.S (2015). Transient-electromagnetic finite-difference time-domain earth modeling over steel infrastructure. *Geophysics*, **80**(2), E147–E162. https://doi.org/10.1190/geo2014-0324.1

Hang Si (2015). TetGen, a Delaunay-Based Quality Tetrahedral Mesh Generator. *ACM Trans. on Mathematical Software*. **41**(2), Article 11, 36 pages. http://doi.acm.org/10.1145/2629697

Hickey, M. S., Treviño III, S., & Everett, M. E. (2015). Detection and Characterization of the Injection of Hydraulic Fracturing Fluid using Ground-Based Controlled-Source Electromagnetics. In *SEG Technical Program Expanded Abstracts* 2015 (pp. 1039–1043). Society of Exploration Geophysicists.

Streich, R. (2016). Controlled-Source Electromagnetic Approaches for Hydrocarbon Exploration and Monitoring on Land. *Surveys in Geophysics*, **37**, 47–80, DOI 10.1007/s10712-015-9336-0